# Resonant x-ray scattering spectra from multipole ordering: Np $M_{4,5}$ edges in $NpO_2$

Tatsuya Nagao
*Faculty of Engineering, Gunma University, Kiryu, Gunma 376-8515, Japan*

Jun-ichi Igarashi
*Faculty of Science, Ibaraki University, Mito, Ibaraki 310-8512, Japan*

(Received 14 June 2005; revised manuscript received 15 August 2005; published 21 November 2005)

We study resonant x-ray scattering (RXS) at Np $M_{4,5}$ edges in the triple-**k** multipole ordering phase in $NpO_2$, on the basis of a localized electron model. We derive an expression for RXS amplitudes to characterize the spectra under the assumption that a rotational invariance (spherical symmetry) is preserved in the Hamiltonian describing the intermediate state of the scattering process. This assumption is justified by the fact that the energies of the crystal electric field and the intersite interaction are smaller than the energy of multiplet structures. This expression is found to be useful to calculate energy profiles taking account of the intra-Coulomb and spin-orbit interactions. Assuming the $\Gamma_8$-quartet ground state, we construct the triple-**k** ground state and analyze the RXS spectra. The energy profiles are calculated in good agreement with the experiment, providing a sound basis to previous phenomenological analyses.

DOI: 10.1103/PhysRevB.72.174421 PACS number(s): 78.70.Ck, 75.25.+z, 75.10.−b, 78.20.Bh

## I. INTRODUCTION

The resonant x-ray scattering (RXS) technique has attracted much attention to study spin and orbital properties of $3d$ transition-metal compounds. RXS at the $K$ edge is described by a second-order optical process that an incident x-ray excites a $1s$ core electron to unoccupied $4p$ states and then the $4p$ electron is recombined with the core hole with emitting x ray in the dipole process ($E1$). It became widely known after the observation of intensities on orbital-ordering superlattice spots at the Mn $K$ edge in $LaMnO_3$.[1] At the earlier stage, the spectra were interpreted as a direct observation of orbital ordering.[2] However, subsequent theoretical studies based on band structure calculations revealed that the spectra are a direct reflection of lattice distortion,[3–5] since the $4p$ state in the intermediate state is influenced not by the orbital ordering of $3d$ electrons but by lattice distortion through hybridization with the $2p$ state at neighboring oxygen sites.

Different from transition-metal compounds, $M_{4,5}$ edges are available for forbidden-reflection Bragg spots in actinide compounds.[6–8] The RXS spectra are more directly reflecting multipole orderings of $5f$ states, since the $E1$ process involves a transition from the $3d$ core to $5f$ states. Each actinide atom usually carries local multipole moments, which can order at low temperatures due to intersite interactions such as exchange interactions. For such localized electron systems, RXS amplitudes are given by summing up contributions at each site. The crystal electric field (CEF) and the intersite interaction can be safely neglected in the intermediate state, because they are much smaller than the intra-atomic Coulomb interaction. Therefore, it may be reasonable to assume that the Hamiltonian describing the intermediate state preserves rotational invariance. Under this assumption, we derive an expression for the RXS amplitude in the $E1$ process to characterize the spectra. Although the expression is essentially the same as the formula by Hannon *et al.*,[9] the present form is useful to calculate energy profiles taking full account of multiplet structures. Using this expression together with a microscopic model, we calculate the RXS spectra in the triple-**k** multipole ordering phase in $NpO_2$.

$NpO_2$ undergoes a second-order phase transition below $T_0=25.5$ K.[10,11] Since Np ions are Kramers ions in the $(5f)^3$ configuration, a magnetic ground state is naturally expected. However, neither Mössbauer spectroscopy[12,13] nor neutron diffraction experiments[14,15] could detect any evidence of a sizable magnetic moment. Actually, the former experiment gave an estimate of the upper limit of the magnitude of the magnetic moment $\sim 0.01\mu_B$, which was too small to explain the effective paramagnetic moment $\sim 2.95\mu_B$.[16] Another complication is that a muon spin relaxation ($\mu$SR) experiment has suggested the low-temperature phase of breaking time-reversal symmetry.[17]

A natural way to reconcile with the above observations is to introduce the higher-rank multipole ordering rather than the dipole moment. Actually, Santini and Amoretti proposed a octupole ordering of $\Gamma_2(xyz)$ symmetry.[18,19] However, this phase can be ruled out because it gives rise to no RXS intensity. Recently, Paixão *et al.* have reported that a longitudinal triple-**k** octupole ordering accounts well for their RXS experiment.[20] The reason for anticipating triple-**k** orderings is that they exclude a crystal distortion or a shift of oxygen positions, which is consistent with the experiment. Experimental data obtained from the $^{17}O$ NMR spectrum, which indicate the existence of two inequivalent oxygen sites, support the occurrence of the triple-**k** octupole ordering phase.[21] Some theoretical works also have lent support to realization of this type of the phase.[22,23]

Assuming the $\Gamma_8$-quartet ground state, we explicitly construct a triple-**k** octupole ordering state within the mean-field approximation at $T=0$. A discussion of the phase transition is beyond the scope of this paper and delegated to Ref. 22. This state is found to simultaneously carry a finite quadrupole moment, which generates the RXS intensity. Since the RXS

 

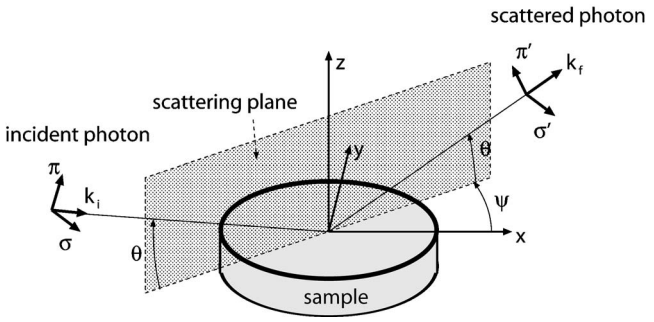


FIG. 1. Geometry of the RXS experiment. Photon with polarization $\sigma$ or $\pi$ is scattered into the state of polarization $\sigma'$ or $\pi'$ at the Bragg angle $\theta$. The azimuthal angle $\psi$ describes the rotation of the sample around the scattering vector $\mathbf{G}$.

amplitudes are characterized by three terms—the scalar, dipole, and quadrupole ones—it is not necessary to assume the existence of the hexadecapole moment instead of the quadrupole moment. We calculate the energy profiles taking full account of multiplet structures in the intermediate state. We obtain spikelike curves at Np $M_4$ edges for smaller values of the core-level width $\Gamma$ as a reflection of multiplet structures. They are found to merge into a single peak with $\Gamma > 1$ eV. The energy profile with $\Gamma \sim 2$ eV seems to agree with the experiment. The azimuthal-angle dependence of the RXS spectra is obtained in agreement with the previous analysis.[20,24] The present analysis provides a sound basis to the previous phenomenological analysis.

The present paper is organized as follows. In Sec. II, we present an expression for the RXS amplitude, which is useful to calculate the energy profiles. In Sec. III, we analyze the RXS spectra in the triple-$\mathbf{k}$ octupole ordering of $NpO_2$ on the basis of a localized electron model. Section IV is devoted to concluding remarks. In the Appendix, we derive the general expression of RXS characterizing energy profiles.

## II. THEORETICAL FRAMEWORK OF RXS

### A. Second-order optical process

In the resonant process, an incident photon with energy $\hbar\omega$, wave vector $\mathbf{k}$, and polarization vector $\boldsymbol{\epsilon}$ excites a core electron to an empty valence shell of the intermediate state; then, the excited electron falls into the core state emitting a photon having the same energy, wave vector $\mathbf{k}'$, and polarization vector $\boldsymbol{\epsilon}'$. For example, at $M_{4,5}$ edges in actinide compounds, a $3d$ core electron is promoted to partially filled $5f$ states at each site by the $E1$ transition. The definition of a geometrical arrangement adopted here is found in Fig. 1. The RXS amplitude is assumed as a sum of contributions from individual ions. Since the dipole matrix element involves a well-localized wave function of core states, the assumption seems quite reasonable. Accordingly, the RXS intensity observed in the experiment may be expressed for the scattering vector $\mathbf{G}(=\mathbf{k}'-\mathbf{k})$ as

$$I(\boldsymbol{\epsilon}', \boldsymbol{\epsilon}, \mathbf{G}, \omega) \propto \left| \frac{1}{\sqrt{N}} \sum_j \mathrm{e}^{-i\mathbf{G}\cdot\mathbf{r}_j} M_j(\boldsymbol{\epsilon}', \boldsymbol{\epsilon}, \omega) \right|^2, \quad (2.1)$$

where $M_j(\boldsymbol{\epsilon}', \boldsymbol{\epsilon}, \omega)$ represents the RXS amplitude at site $j$ with $N$ being the number of sites. For the $E1$ transition, it is expressed as[9,25–27]

$$M_j(\boldsymbol{\epsilon}', \boldsymbol{\epsilon}, \omega) = \sum_{\alpha', \alpha} \epsilon'_\alpha \epsilon_{\alpha'} \sum_\Lambda \frac{\langle \psi_0 | x_{\alpha,j} | \Lambda \rangle \langle \Lambda | x_{\alpha',j} | \psi_0 \rangle}{\hbar\omega - (E_\Lambda - E_0) + i\Gamma}, \quad (2.2)$$

where the dipole operators $x_{\alpha,j}$'s are defined as $x_{1,j}=x_j$, $x_{2,j}=y_j$, and $x_{3,j}=z_j$ in the coordinate frame fixed to the crystal axes with the origin located at the center of site $j$. The $|\psi_0\rangle$ represents the ground state with energy $E_0$, while $|\Lambda\rangle$ represents the intermediate state with energy $E_\Lambda$. The $\Gamma$ describes the lifetime broadening width of the core hole.

### B. Energy profiles

In localized models, the ground state and intermediate state at each site are well specified by the eigenfunctions of the angular momentum operator, $|J,m\rangle$. The CEF and the intersite interaction usually lifts the degeneracy in the ground state. Thus the ground state at site $j$ may be expressed as $|\psi_0\rangle_j = \Sigma_m c_j(m)|J,m\rangle$. On the other hand, in the intermediate state, we can neglect the CEF and the intersite interaction in a good approximation, since their energies are much smaller than the intra-atomic Coulomb interaction and the spin-orbit interaction (SOI) which give rise to the multiplet structure. Thus the Hamiltonian describing the intermediate state preserves the spherical symmetry. Under the assumption, as derived in the Appendix, we obtain a general expression of the scattering amplitude at site $j$:

$$M_j(\boldsymbol{\epsilon}', \boldsymbol{\epsilon}, \omega) = \alpha_0(\omega) \boldsymbol{\epsilon}' \cdot \boldsymbol{\epsilon} - i\alpha_1(\omega)(\boldsymbol{\epsilon}' \times \boldsymbol{\epsilon}) \cdot \langle \psi_0 | \mathbf{J} | \psi_0 \rangle + \alpha_2(\omega) \sum_\nu P_\nu(\boldsymbol{\epsilon}', \boldsymbol{\epsilon}) \langle \psi_0 | z_\nu | \psi_0 \rangle, \quad (2.3)$$

where

$$z_1 \equiv Q_{x^2-y^2} = \frac{\sqrt{3}}{2}(J_x^2 - J_y^2), \quad (2.4a)$$

$$z_2 \equiv Q_{3z^2-r^2} = \frac{1}{2}[3J_z^2 - J(J+1)], \quad (2.4b)$$

$$z_3 \equiv Q_{yz} = \frac{\sqrt{3}}{2}(J_y J_z + J_z J_y), \quad (2.4c)$$

$$z_4 \equiv Q_{zx} = \frac{\sqrt{3}}{2}(J_z J_x + J_x J_z), \quad (2.4d)$$

$$z_5 \equiv Q_{xy} = \frac{\sqrt{3}}{2}(J_x J_y + J_y J_x) \quad (2.4e)$$

and

$$P_1(\boldsymbol{\epsilon}', \boldsymbol{\epsilon}) = \frac{\sqrt{3}}{2}(\epsilon'_x \epsilon_x - \epsilon'_y \epsilon_y), \quad (2.5a)$$

$$P_2(\boldsymbol{\epsilon}', \boldsymbol{\epsilon}) = \frac{1}{2}(2\epsilon'_z \epsilon_z - \epsilon'_x \epsilon_x - \epsilon'_y \epsilon_y), \quad (2.5b)$$

$$P_3(\epsilon',\epsilon)=\frac{\sqrt{3}}{2}(\epsilon'_y\epsilon_z+\epsilon'_z\epsilon_y), \tag{2.5c}$$

$$P_4(\epsilon',\epsilon)=\frac{\sqrt{3}}{2}(\epsilon'_z\epsilon_x+\epsilon'_x\epsilon_z), \tag{2.5d}$$

$$P_5(\epsilon',\epsilon)=\frac{\sqrt{3}}{2}(\epsilon'_x\epsilon_y+\epsilon'_y\epsilon_x). \tag{2.5e}$$

Here we have suppressed the dependence on $j$ on the right-hand side of Eq. (2.3). The energy profiles are given by only three functions $\alpha_0(\omega)$, $\alpha_1(\omega)$, and $\alpha_2(\omega)$, whose expressions are explicitly given in the Appendix.

Several facts are immediately deduced from Eq. (2.3). First, since the scalar, dipole, and quadrupole terms exhaust the amplitude, the octupole ordering alone does not give rise to the RXS amplitude. Second, the choice of the CEF parameters in the ground state does not affect the shape of energy profiles $\alpha_0(\omega)$, $\alpha_1(\omega)$, and $\alpha_2(\omega)$, although it affects the expectation values of dipole and/or quadrupole operators. Third, $\alpha_0(\omega)$ has no contribution to the forbidden Bragg spots in the antiferro-type structure. In order to calculate the energy profiles, however, we need to know explicitly wave functions of the intermediate state, which are discussed in the next section.

### C. Absorption coefficient

Within the $E1$ transition, the absorption coefficient is given by

$$A(\omega)\propto\sum_j\sum_\alpha\sum_\Lambda|\langle\Lambda|x_{\alpha,j}|\psi_0\rangle|^2\frac{\Gamma/\pi}{(\hbar\omega-E_\Lambda+E_0)^2+\Gamma^2}, \tag{2.6}$$

where $|\Lambda\rangle$ with energy $E_\Lambda$ represents the final state, which is equivalent to the intermediate state of RXS. A comparison of Eq. (2.6) with Eq. (2.2) leads to

$$A(\omega)\propto-\mathrm{Im}\,\alpha_0(\omega), \tag{2.7}$$

where Im $X$ denotes the imaginary part of $X$.

## III. RXS SPECTRA FROM $NpO_2$

### A. Quartet ground state

$NpO_2$ has the $CaF_2$-type structure ($F_{m\bar{3}m}$) with a lattice constant $a=5.431$ Å at room temperature, as schematically shown in Fig. 2.[10] Np ions are tetravalent in $NpO_2$, as confirmed by the isomer shift in Mössbauer spectra[12] and by the neutron diffraction experiment.[28] In a localized description, each Np ion is in the $(5f)^3$-configuration. The Hamiltonian of Np ions consists of the intra-atomic Coulomb interaction between $5f$ electrons in addition to the SOI of $5f$ electrons. The Slater integrals for the Coulomb interaction and the SOI parameters are evaluated within the Hatree-Fock approximation[29] (HFA) and are listed in Table I. These values are usually reduced by many-body effects[30]—for example, the intra-atomic configuration interaction. The reduction of the anisotropic part is known to be small; we use the values multiplied by a factor of 0.8. The screened value of the isotropic part $F^0$ is not known, but an accurate value is not necessary for the present purpose, because it is absorbed into the $M$-edge energy in the spectra. Within the HFA, the ground state has tenfold degeneracy corresponding to the $J=9/2$ multiplet. The choice of the multiplying factors does not alter this conclusion.[31] Note that these states of $J=9/2$ are slightly deviated from those of the perfect Russell-Saunders (RS) coupling scheme with $L=6$ and $S=3/2$ due to the presence of the strong SOI. For instance, $\mathbf{L}^2$ and $\mathbf{S}^2$ take values 39.752 and 3.237 respectively, compared to the RS values 42 and 3.75.

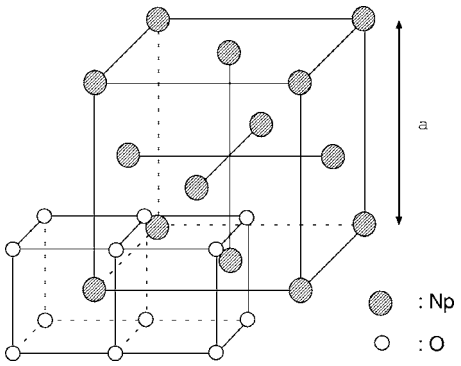


FIG. 2. Crystal structure of $NpO_2$. Gray circles denote Np ions and open circles represent O ions.

In crystal, the tenfold degeneracy is lifted by the CEF. Under cubic symmetry, the CEF Hamiltonian $H_{CEF}$ may be expressed as

$$H_{CEF}=B_4(O_4^0+5O_4^4)+B_6(O_6^0-21O_6^4), \tag{3.1}$$

where $O_k^q$'s represent the Stevens operator equivalence. Thereby the degenerate levels are split into one doublet $\Gamma_6$ and two quartets $\Gamma_8^{(1)}$ and $\Gamma_8^{(2)}$. The level scheme has been analyzed by the inelastic neutron scattering, which yields an estimate of CEF parameters as $B_4=-3.03\times10^{-2}$ meV and $B_6=2.36\times10^{-4}$ meV.[32,33]

The lowest levels are given by the $\Gamma_8^{(2)}$, which is separated about 55 meV from another quartet $\Gamma_8^{(1)}$. Diagonalizing Eq. (3.1), we obtain the bases of the lowest quartet as

TABLE I. Slater integrals and spin-orbit interaction parameters in the $(3d)^{10}(5f)^3$ configuration within the HF approximation (in units of eV) (Ref. 29).

| $F^k(3d,3d)$ | $F^k(3d,5f)$ | $F^k(5f,5f)$ | $G^k(3d,5f)$ |
|---|---|---|---|
| $F^0$ 180.1 | | $F^0$ 19.61 | |
| $F^2$ 92.04 | | $F^2$ 9.909 | |
| $F^4$ 59.28 | | $F^4$ 6.491 | |
| | | $F^6$ 4.769 | |
| $\zeta_{3d}=76.254$ | $\zeta_{5f}=0.298$ | | |

$$|+\uparrow\rangle = c_1\left|+\frac{9}{2}\right\rangle + c_2\left|+\frac{1}{2}\right\rangle + c_3\left|-\frac{7}{2}\right\rangle, \tag{3.2}$$

$$|+\downarrow\rangle = c_1\left|-\frac{9}{2}\right\rangle + c_2\left|-\frac{1}{2}\right\rangle + c_3\left|+\frac{7}{2}\right\rangle, \tag{3.3}$$

$$|-\uparrow\rangle = c_4\left|+\frac{5}{2}\right\rangle + c_5\left|-\frac{3}{2}\right\rangle, \tag{3.4}$$

$$|-\downarrow\rangle = c_4\left|-\frac{5}{2}\right\rangle + c_5\left|+\frac{3}{2}\right\rangle, \tag{3.5}$$

with $c_1=0.2757$, $c_2=-0.4483$, $c_3=0.8503$, $c_4=-0.9751$, and $c_5=0.2216$. State $|m\rangle$ denotes the eigenstate with $J_z=m$. Symbols $\tau(=\pm)$ and $\sigma(=\uparrow,\downarrow)$ are introduced to represent the state $|\tau,\sigma\rangle$, which distinguish non-Kramers and Kramers pairs, respectively.

### B. Triple-k structure

The fourfold degeneracy in the ground $\Gamma_8^{(2)}$ quartet may be lifted by the intersite interaction, giving rise to nonvanishing expectation values of multipole moments. Actually, several experiments tell us that the time-reversal symmetry is broken with nearly zero dipole moment in the ordered phase below $T_0=25.5$ K.[17,21] These observations lead Santini and Amoretti to propose the antiferro-octupole ordering of $T_{xyz}$ type $[T_{xyz}\equiv(\sqrt{15}/6)\overline{J_xJ_yJ_z}]$.[18,19] Here the overbar on operators means symmetrization—for example, $\overline{J_xJ_y^2}=J_xJ_y^2+J_yJ_xJ_y+J_y^2J_x$.[34] Unfortunately, this phase would not give rise to the RXS intensities observed in the experiments.

An important observation is that no external distortion from cubic structure exists in the ordered phase; that is, the unit cell remains cubic below $T_0$. This leads us to consider the triple-**k** ordering, since it allows the crystal to keep the cubic symmetry. As schematically shown in Fig. 3, the triple-**k** structure is defined by all three members of the star of **k** $=\langle 001\rangle$ simultaneously present on each site of the lattice. The order parameter vector of the longitudinal (transverse) ordering is composed of three longitudinal (transverse) waves with different **k**'s. There are four sublattices 1, 2, 3, and 4 at (0,0,0), $(\frac{1}{2},\frac{1}{2},0)$, $(0,\frac{1}{2},\frac{1}{2})$, and $(\frac{1}{2},0,\frac{1}{2})$, respectively.

#### 1. Octupole ordering

We start by the octupole ordering of $\Gamma_{5u}$ type proposed by Paixão *et al.*[20] The corresponding octupole operators are defined by

$$T_x^\beta = \frac{\sqrt{15}}{6}\overline{J_x(J_y^2-J_z^2)}, \tag{3.6a}$$

$$T_y^\beta = \frac{\sqrt{15}}{6}\overline{J_y(J_z^2-J_x^2)}, \tag{3.6b}$$

$$T_z^\beta = \frac{\sqrt{15}}{6}\overline{J_z(J_x^2-J_y^2)}. \tag{3.6c}$$

We first introduce the operators

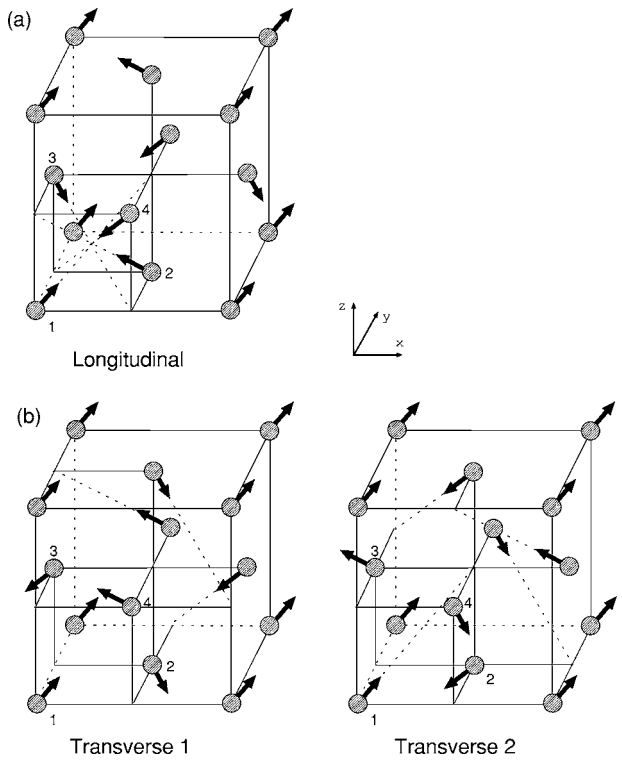


FIG. 3. Triple-**k** antiferro-type arrangements: (a) a longitudinal pattern and (b) two transverse patterns (1 and 2). Arrows indicate vectors $(\langle J_x\rangle,\langle J_y\rangle,\langle J_z\rangle)$, $(\langle Q_{yz}\rangle,\langle Q_{zx}\rangle,\langle Q_{xy}\rangle)$, and $(\langle T_x^\beta\rangle,\langle T_y^\beta\rangle,\langle T_z^\beta\rangle)$, corresponding to the dipole, quadrupole, and octupole orderings, respectively. Numbers 1, 2, 3, and 4 specify the sublattices. Oxygen ions are omitted.

$$T_p = \begin{cases} \dfrac{1}{\sqrt{3}}(T_x^\beta + T_y^\beta + T_z^\beta) & \text{for } p=111, \\ \dfrac{1}{\sqrt{3}}(T_x^\beta - T_y^\beta - T_z^\beta) & \text{for } p=1\bar{1}\bar{1}, \\ \dfrac{1}{\sqrt{3}}(-T_x^\beta + T_y^\beta - T_z^\beta) & \text{for } p=\bar{1}1\bar{1}, \\ \dfrac{1}{\sqrt{3}}(-T_x^\beta - T_y^\beta + T_z^\beta) & \text{for } p=\bar{1}\bar{1}1. \end{cases} \tag{3.7}$$

Note here that the overbar appearing in the subscript $p$ denotes the negative direction, not symmetrization. Each $T_p$ operator has eigenvalues $\pm t_1(t_1=-6.102)$ and doubly degenerated 0. The eigenstates of eigenvalues $\pm t_1$ are connected to each other by the time-reversal operation and so are two degenerate states of eigenvalue 0. For example, the eigenstate of eigenvalue $-t_1$ for $T_{111}$ is explicitly written as

$$|-t_1\rangle = \frac{1}{2}e^{i(\theta_{111}-\pi/2)}[|+\uparrow\rangle + e^{-i\pi/4}|+\downarrow\rangle] - \frac{1}{2}[|-\uparrow\rangle + e^{i3\pi/4}|-\downarrow\rangle], \tag{3.8}$$

with $\theta_{111}$ being an angle between vector (1,1,1) and the $z$

axis—that is, $\cos\theta_{111}=\sqrt{1/3}$ and $\sin\theta_{111}=\sqrt{2/3}$. Using the eigenstates as bases, $T_p$ is represented as

$$T_p=\begin{pmatrix} -t_1 & 0 & 0 & 0 \\ 0 & +t_1 & 0 & 0 \\ 0 & 0 & 0 & 0 \\ 0 & 0 & 0 & 0 \end{pmatrix}. \tag{3.9}$$

Now we analyze the orders shown in Fig. 3. Within the mean-field approximation, the single-site Hamiltonian may be of the form $H_{\text{single}}=hT_p$, with $T_p=T_{111}$, $T_{1\bar{1}\bar{1}}$, $T_{\bar{1}1\bar{1}}$, and $T_{\bar{1}\bar{1}1}$ for sublattices 1, 3, 4, and 2, in the longitudinal order; $T_p=T_{111}$, $T_{1\bar{1}\bar{1}}$, $T_{\bar{1}1\bar{1}}$, and $T_{\bar{1}\bar{1}1}$, for sublattices 1, 2, 3, and 4; and 1, 4, 2, and 3, in the transverse order 1 and 2, respectively. Th $h$ represents the mean field, which may be expressed as $h=\alpha\langle T_p\rangle$ with $\alpha$ a constant. We construct the ground state by assigning either of eigenstates of $\pm t_1$ to each sublattice; which eigenstate is relevant depends on the sign of acting mean field. The eigenstates make the order parameter vector $(\langle T_x^\beta\rangle,\langle T_y^\beta\rangle,\langle T_z^\beta\rangle)$ point to the $\pm p$ direction for $\pm t_1$. Therefore, the assignment of the eigenstates is consistent with the assumed order. Note that the wave function at each site is different from that assumed by Lovesey *et al.*, who considered the state deviating from the $\Gamma_8$ quartet.[35]

Introducing the quadrupole operators

$$Q_p=\begin{cases} \frac{1}{\sqrt{3}}(Q_{yz}+Q_{zx}+Q_{xy}) & \text{for } p=111, \\ \frac{1}{\sqrt{3}}(Q_{yz}-Q_{zx}-Q_{xy}) & \text{for } p=1\bar{1}\bar{1}, \\ \frac{1}{\sqrt{3}}(-Q_{yz}+Q_{zx}-Q_{xy}) & \text{for } p=\bar{1}1\bar{1}, \\ \frac{1}{\sqrt{3}}(-Q_{yz}-Q_{zx}+Q_{xy}) & \text{for } p=\bar{1}\bar{1}1, \end{cases} \tag{3.10}$$

we can similarly construct the quadrupole ordering state by assigning them to each sublattice in the same way as for octupole orderings. Since $Q_p$'s and $T_p$'s are simultaneously diagonalized because of commuting with each other, $Q_p$ could be represented as

$$Q_p=\begin{pmatrix} -q_1 & 0 & 0 & 0 \\ 0 & -q_1 & 0 & 0 \\ 0 & 0 & +q_1 & 0 \\ 0 & 0 & 0 & +q_1 \end{pmatrix}, \tag{3.11}$$

with $q_1=-8.273$.

According to the mean-field analysis at $T=0$, the octupole-ordered ground state can be stabilized through the octupole-octupole intersite interaction. Each Np ion is in the eigenstate of the eigenvalue $-t_1$ (or $t_1$). Since the state is also the eigenstate of the eigenvalue $-q_1$, the quadrupole ordering is simultaneously realized. On the other hand, if the quadrupole order is primary, each Np ion is in the eigenstate of the eigenvalue $-q_1$ or $q_1$. For the case of eigenvalue $-q_1$, two eigenstates are degenerate and give eigenvalues $-t_1$ and $t_1$ to the octupole moment $T_p$, and thereby the net octupole moment becomes zero. For the case of $q_1$, two eigenstates are also degenerate and give the eigenvalue 0 to $T_p$. In either case, the quadrupole order carries no octupole order. Since the double degeneracy remains in this phase, it must be lifted at lower temperatures by realizing an octupole-ordered phase. Considering the experimental facts that the time-reversal symmetry is broken and the phase transition takes place only once, we conclude that the primary order parameter is the octupole order.

#### *2. Dipole ordering*

Although the dipole ordering is ruled out in $NpO_2$, it may be interesting to discuss here what happens in the dipole ordering. Such kind of ordering pattern may be found in $UO_2$ and $U_{0.75}Np_{0.25}O_2$.[36]

Introducing the dipole operators

$$J_p=\begin{cases} \frac{1}{\sqrt{3}}(J_x+J_y+J_z) & \text{for } p=111, \\ \frac{1}{\sqrt{3}}(J_x-J_y-J_z) & \text{for } p=1\bar{1}\bar{1}, \\ \frac{1}{\sqrt{3}}(-J_x+J_y-J_z) & \text{for } p=\bar{1}1\bar{1}, \\ \frac{1}{\sqrt{3}}(-J_x-J_y+J_z) & \text{for } p=\bar{1}\bar{1}1, \end{cases} \tag{3.12}$$

we can construct the dipole ordering state by assigning them to each sublattice in the same way as in the octupole ordering. Note that $J_p$ and $Q_p$ are simultaneously diagonalized, because both operators commute with each other. Within the bases of simultaneous eigenstates of $J_p$ and $Q_p$, the relevant operators are represented as

$$J_p=\begin{pmatrix} -j_1 & 0 & 0 & 0 \\ 0 & +j_1 & 0 & 0 \\ 0 & 0 & -j_2 & 0 \\ 0 & 0 & 0 & +j_2 \end{pmatrix}, \tag{3.13}$$

$$Q_p=\begin{pmatrix} -q_1 & 0 & 0 & 0 \\ 0 & -q_1 & 0 & 0 \\ 0 & 0 & +q_1 & 0 \\ 0 & 0 & 0 & +q_1 \end{pmatrix}, \tag{3.14}$$

$$T_p=\begin{pmatrix} 0 & -t_1 & 0 & 0 \\ -t_1 & 0 & 0 & 0 \\ 0 & 0 & 0 & 0 \\ 0 & 0 & 0 & 0 \end{pmatrix}, \tag{3.15}$$

where $j_1=3.27$ and $j_2=0.18$ with parameters given in $NpO_2$. The magnetic moment is evaluated on either of eigenstates of $\pm j_1$: $\langle L_p+2S_p\rangle=2.48$ ($L_p$ and $S_p$ are defined as in the same way as $J_p$).

In the dipole ordering, the ground state is given by assigning one of the eigenstates of $J_p$'s to each sublattice. Since $j_1$

TABLE II. RXS amplitudes in triple-**k** ordering, for $\mathbf{G}=(hh\ell)$ with $h+\ell=$odd. Longitudinal, transverse 1, and transverse 2 correspond to the ordering patterns shown in Fig. 3.

| | RXS amplitude | | |
|---|---|---|---|
| | Longitudinal | Transverse 1 | Transverse 2 |
| Dipole | $-i\alpha_1(\omega)\langle\psi_0\|J_z\|\psi_0\rangle(\epsilon'\times\epsilon)_z$ $+\alpha_2(\omega)\langle\psi_0\|Q_5\|\psi_0\rangle P_5(\epsilon',\epsilon)$ | $-i\alpha_1(\omega)\langle\psi_0\|J_x\|\psi_0\rangle(\epsilon'\times\epsilon)_x$ $+\alpha_2(\omega)\langle\psi_0\|Q_3\|\psi_0\rangle P_3(\epsilon',\epsilon)$ | $-i\alpha_1(\omega)\langle\psi_0\|J_y\|\psi_0\rangle(\epsilon'\times\epsilon)_y$ $+\alpha_2(\omega)\langle\psi_0\|Q_4\|\psi_0\rangle P_4(\epsilon',\epsilon)$ |
| Quadrupole | $\alpha_2(\omega)\langle\psi_0\|Q_5\|\psi_0\rangle P_5(\epsilon',\epsilon)$ | $\alpha_2(\omega)\langle\psi_0\|Q_3\|\psi_0\rangle P_3(\epsilon',\epsilon)$ | $\alpha_2(\omega)\langle\psi_0\|Q_4\|\psi_0\rangle P_4(\epsilon',\epsilon)$ |
| Octupole | $\alpha_2(\omega)\langle\psi_0\|Q_5\|\psi_0\rangle P_5(\epsilon',\epsilon)$ | $\alpha_2(\omega)\langle\psi_0\|Q_3\|\psi_0\rangle P_3(\epsilon',\epsilon)$ | $\alpha_2(\omega)\langle\psi_0\|Q_4\|\psi_0\rangle P_4(\epsilon',\epsilon)$ |

is much larger than $j_2$, the ground state is likely to be either of eigenstates of $\pm j_1$. From Eqs. (3.14) and (3.15), this state gives the finite average value of the quadrupole moment but no average value of the octupole moment. If this state is mixed with another eigenstate, the new state has a finite average value of the octupole moment and thereby may gain a negative energy of the octupole-octupole interaction. But the mixing of another eigenstate causes an increase of the dipole-dipole energy. If the dipole-dipole interaction is dominant, the latter would be large and no octupole order is induced at $T=0$. Note that, if the quadrupole ordering is primary, no dipole moment is induced, because the doubly degenerate eigenstates of $Q_p$ are the eigenstates of $\pm j_1$ of $J_p$. The same discussion as in the case of the octupole ordering can be applied.

### C. RXS spectra

Irrespective of whether the octupole or quadrupole ordering is realized, RXS amplitudes are generated at each site, according to Eq. (2.3). They are proportional to $q_1\alpha_2(\omega)\times(P_3+P_4+P_5)$ for the simultaneous eigenstate of $T_{111}$ and $Q_{111}$, to $q_1\alpha_2(\omega)(P_3-P_4-P_5)$ for the simultaneous eigenstate of $T_{1\bar{1}\bar{1}}$ and $Q_{1\bar{1}\bar{1}}$, to $q_1\alpha_2(\omega)(-P_3+P_4-P_5)$ for the simultaneous eigenstate of $T_{\bar{1}1\bar{1}}$ and $Q_{\bar{1}1\bar{1}}$, and to $q_1\alpha_2(\omega)(-P_3-P_4+P_5)$ for the simultaneous eigenstate of $T_{\bar{1}\bar{1}1}$ and $Q_{\bar{1}\bar{1}1}$. On the scattering vector $\mathbf{G}=(hh\ell)$ with $h+\ell=$odd, these amplitudes are summed up with a positive sign for sublattices 1 and 2 and with a negative sign for sublattices 3 and 4. Therefore, the total RXS amplitude becomes proportional to $q_1\alpha_2(\omega)P_5$ for the longitudinal order, while they are proportional to $q_1\alpha_2(\omega)P_3$ and $q_1\alpha_2(\omega)P_4$ for the two transverse orders. Note that a similar analysis is applied to the dipole ordering. In this case, both the dipole and quadrupole terms contribute to the amplitude. These results are summarized in Table II. For the transverse case, our present treatment could be extended applying to the RXS spectra detected at Np $M_4$ edges in $U_{0.75}Np_2O_2$.[36] In this compound, the spectra may be interpreted as a consequence brought about by the transverse type of triple-**k** antiferromagnetic (AFM) ordering driven by the same ordering pattern at U sites.

Polarization dependences become particularly simple for $\mathbf{G}=(00\ell)(\ell=$odd) in the octupole and quadrupole orderings. They are explicitly written in the scattering geometry shown in Fig. 1 as $P_3=0$, $P_4=0$, and $P_5=(\sqrt{3}/2)\sin 2\psi$ in the $\sigma$-$\sigma'$ channel, while $P_3=(\sqrt{3}/2)\cos\theta\cos\psi$, $P_4=(\sqrt{3}/2)\cos\theta\sin\psi$, $P_5=(\sqrt{3}/2)\sin\theta\cos 2\psi$ in the $\sigma$-$\pi'$ channel. Figure 4 shows the azimuthal angle dependence of the spectra $\mathbf{G}=(003)$ in comparison with the experiment.[20,24] The experimental data are well fitted by $\sin^2 2\psi$ in the $\sigma$-$\sigma'$ channel and $\sin^2\theta\cos^2 2\psi$ in the $\sigma$-$\pi'$ channel. The two transverse orders cannot reproduce the experimental curves, as seen from panel (b). Paixão *et al.* and Caciuffo *et al.* analyzed their experimental data and concluded that the longitudinal order gives rise to this dependence.[20,24] The present analysis confirms their result. Note that, based on a group theoretical point of view, Nikolaev and Michel have obtained the same result.[37]

Now we discuss the energy profiles. In order to calculate them, we need the wave functions in the intermediate state. We first evaluate the Slater integrals for the Coulomb interaction and the SOI parameters within the HFA, which are shown in Table III. These values are reduced by taking account of screening effects. The reduction factors are set the same as in the ground state. The Hamiltonian of the intermediate state, consisting of the full intra-atomic Coulomb interactions between $5f$-$5f$, $5f$-$3d$, and $3d$-$3d$ electrons as well as

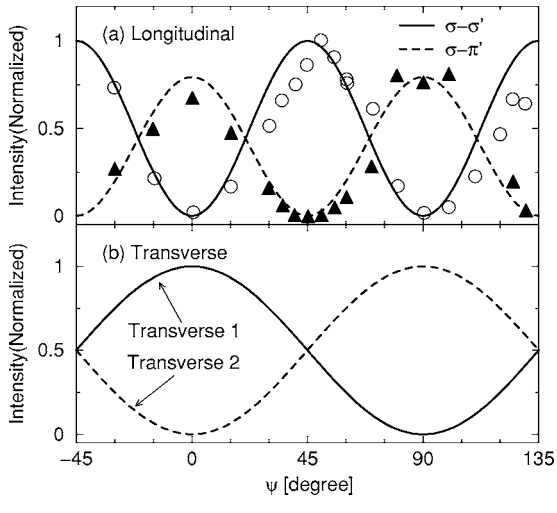


FIG. 4. Azimuthal angle dependence of the RXS spectra from the triple-**k** AFO phases with $\mathbf{G}=(003)$. (a) Longitudinal ordering. The open circles and solid triangles are experimental data, and the solid and dashed lines are the calculated results, in the $\sigma$-$\sigma'$ and $\sigma$-$\pi'$ channels, respectively (Ref. 24). (b) Transverse orderings in the $\sigma$-$\pi'$ channel. No RXS signal is expected from these orders in the $\sigma$-$\sigma'$ channel. The solid and dashed lines are the calculated results for the two transverse orders.

TABLE III. Slater integrals and spin-orbit interaction parameters in the $(3d)^9(5f)^4$ configuration within the HFA (in units of eV) (Ref. 29).

| $F^k(3d,3d)$ | | $F^k(3d,5f)$ | | $F^k(5f,5f)$ | | $G^k(3d,5f)$ | |
|---|---|---|---|---|---|---|---|
| $F^0$ | 181.0 | $F^0$ | 29.13 | $F^0$ | 20.54 | $G^1$ | 2.158 |
| $F^2$ | 92.62 | $F^2$ | 2.749 | $F^2$ | 10.39 | $G^3$ | 1.306 |
| $F^4$ | 59.67 | $F^4$ | 1.281 | $F^4$ | 6.943 | $G^5$ | 0.914 |
| | | | | $F^6$ | 5.017 | | |
| $\zeta_{3d}$=77.278 | | $\zeta_{5f}$=0.339 | | | | | |

the SOI of $5f$ and $3d$ electrons, is represented by $1001 \times (2j_d+1)$ microscopic states with the total angular momentum of the core hole $j_d=3/2$ and $5/2$ corresponding to the $M_4$ and $M_5$ edges, respectively. Diagonalizing the Hamiltonian matrix, we obtain multiplet structures in the intermediate state. The $\alpha_2(\omega)$ is calculated by using Eq. (A8).

The energy profile is proportional to $|\alpha_2(\omega)|^2$ in the octupole ordering phase. The calculated spectra around $M_4$ and $M_5$ edges are displayed with several choices of $\Gamma$ values in Fig. 5. The origin of the energy is adjusted such that the peak of the RXS spectrum is located at the experimental peak position. Since there is no reliable estimation for the $\Gamma$ value, we choose three typical values $\Gamma=0.01$, 0.5, and 2.0 eV. The spikelike curves with $\Gamma=0.01$ eV directly reflect the multiplet splittings of the intermediate states. For the $M_4$ edge, the choice $\Gamma=0.5$ eV makes a multipeak-structure line shape. It merges into a single-peak structure around $\Gamma \simeq 1.0$ eV. The choice $\Gamma=2.0$ eV corresponds to one of better fittings with the experimental line shape.[20,24] The core-level energy is adjusted such that the calculated peak at the $M_4$ edge with $\Gamma=2$ eV coincides with the experimental one. Paixão *et al.* reported that the line shape is well fitted by a Lorentzian-squared rather than a Lorentzian one.[20] As shown above, the line shape is basically determined by the multiplet structure, which is smeared by the lifetime broadening. Whether it looks Lorentzian squared or Lorentzian seems unimportant. As for the spectra at the $M_5$ edge, their shape depends rather sensitively on the value of $\Gamma$ compared to that at the $M_4$ edge.

The energy profile in the dipole ordering is given by the sum of the dipole and quadrupole terms. However, $|\alpha_1(\omega)|^2$ is about two orders of magnitude larger than $|\alpha_2(\omega)|^2$. For instance, $|\alpha_1(\omega)|^2 \sim 192 \times |\alpha_2(\omega)|^2$ when $\Gamma=2.0$ eV. Thus the dipole term usually dominates the quadrupole term. Although the dipole ordering is ruled out from experiments, we show $|\alpha_1(\omega)|^2$ in Fig. 6 as a reference. The peak at the $M_4$ edge with $\Gamma=2$ eV is at 3847.5 eV, 0.7 eV higher than the peak position of $|\alpha_2(\omega)|^2$. Note that the spectral shape at the $M_5$ edge depends on $\Gamma$ more sensitively than that at the $M_4$ edge. For $\mathbf{G}=(hh\ell)$ with $h+\ell=$odd, only $|\alpha_2(\omega)|^2$ survives in the $\sigma$-$\sigma'$ channel. Then, $|\alpha_1(\omega)|^2$ and $|\alpha_2(\omega)|^2$ may explain the RXS spectra observed at Np $M_4$ edge from $U_{0.75}Np_{0.25}O_2$ with $\mathbf{G}=(112)$ in the $\sigma$-$\pi'$ and $\sigma$-$\sigma'$ channels, respectively.[36]

### D. Absorption coefficient

The absorption coefficient is proportional to $-\mathrm{Im}\,\alpha_0(\omega)$. We calculate $\alpha_0(\omega)$ from Eq. (A4) in the same way as in the calculation of $\alpha_1(\omega)$ and $\alpha_2(\omega)$. The calculated results are shown in Fig. 7 at the $M_4$ and $M_5$ edges. The present calculation confirms the previous multiplet calculation by Lovesey *et al.*, in which $-\mathrm{Im}\,\alpha_0(\omega)$ has been calculated at the $M_4$ edge for $\Gamma=0.7$ eV.[35] With increasing values of $\Gamma$, the multiplet structure merges into a single peak. The peak position at the $M_4$ edge with $\Gamma=2$ eV is about 0.35 eV higher than that in $|\alpha_2(\omega)|^2$.

## IV. CONCLUDING REMARKS

In this paper, we have studied the RXS spectra at the Np $M_{4,5}$ edges in the triple-**k** multipole ordering phase of $NpO_2$, on the basis of a localized electron model. We have derived

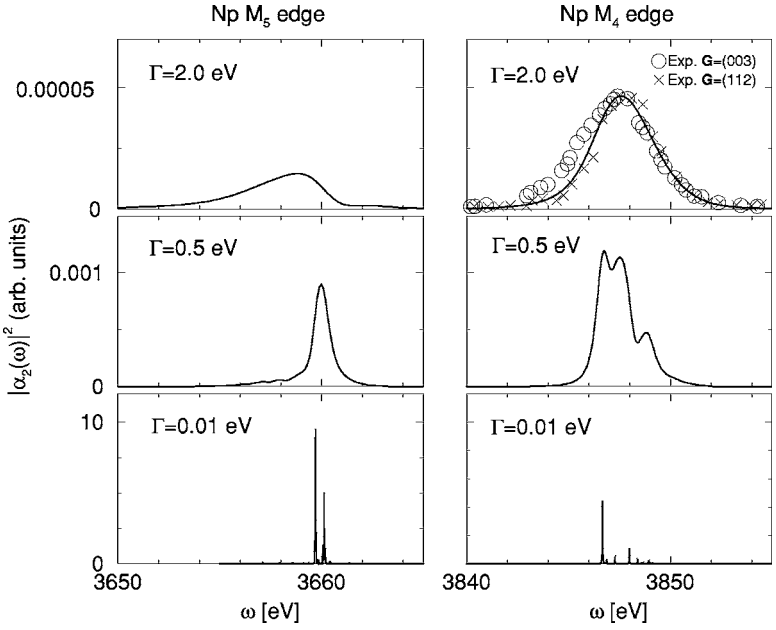


FIG. 5. Energy profiles $|\alpha_2(\omega)|^2$ at the Np $M_4$ (right panels) and $M_5$ (left panels) edges. The lines represent the calculated results for $\Gamma=0.01$, 0.5, and 2.0 eV, respectively, from bottom to top panels. In the top right panel, the open circles and crosses are experimental data in $NpO_2$ (Refs. 20 and 24). The peak heights of them are adjusted to that of the calculated value.

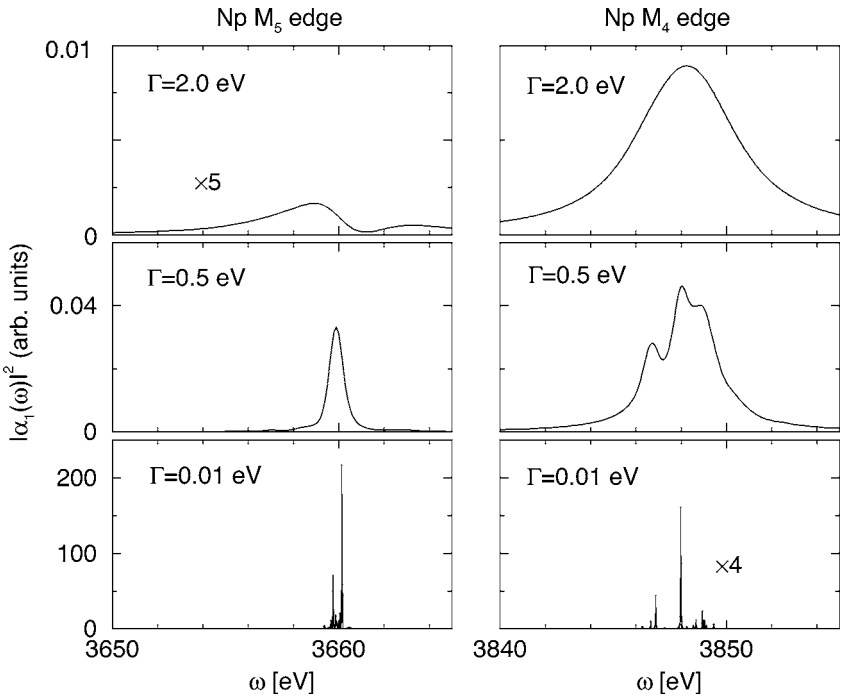


FIG. 6. Energy profiles $|\alpha_1(\omega)|^2$ at the Np $M_4$ (right panels) and $M_5$ (left panels) edges. The lines represent the calculated results for $\Gamma=0.01$, 0.5, and 2.0 eV, respectively, from bottom to top panels.

an expression of scattering amplitudes in the $E1$ process, assuming that the rotational invariance is preserved in the Hamiltonian describing the intermediate state of the scattering process. This is a reasonable assumption when the multiplet energy is larger than those of the CEF and the intersite interaction. On the basis of this expression, we have analyzed the RXS spectra in $NpO_2$. Assuming the $\Gamma_8$-quartet ground state, we have constructed the triple-**k** ordering ground state. The energy profiles have been calculated by taking full account of the multiplet structure in the intermediate state, in agreement with the experiment.

RXS signals on multipole ordering superlattice spots have also been observed and analyzed at $L_{2,3}$ edges of rare-earth metals in their compounds such as $CeB_6$ and $DyB_2C_2$.[38–45] The intermediate state is created by the transition from the $2p$ core to $5d$ states. Since the $5d$ states are considerably delocalized with forming energy bands, the assumption that the intermediate Hamiltonian preserves the rotational invariance becomes less accurate. An extension of the formula is left in future study.

## ACKNOWLEDGMENTS

We thank M. Yokoyama and M. Takahashi for valuable discussions. This work was partially supported by a Grant-in-Aid for Scientific Research from the Ministry of Education, Science, Sports and Culture, Japan.

## APPENDIX: DERIVATION OF EQ. (2.3)

We derive a general expression of RXS amplitude under the assumption that the Hamiltonian describing the intermediate state keeps the rotational symmetry at each site. The following derivation emphasizes the multiplet structure in the intermediate state. Thereby it is more general than the previous analyses, in which the fast collision approximation was adopted by replacing the multiplets with a single level.[9,46,47] A part of the results found in this appendix were used in Ref. 48 when we analyzed the RXS spectra form $URu_2Si_2$.

Let the core hole be created at site $j$ in the intermediate state. We express the intermediate state as $|\Lambda\rangle=|J',M,i\rangle$, where the magnitude $J'$ and the magnetic quantum number $M$ of total angular momentum (including a core-hole angular momentum) are good quantum numbers. To distinguish multiplets having the same $J'$ value but having the different energy, we introduce the index $i$. Defining $M_{\alpha\alpha'}$ by $M_j(\boldsymbol{\epsilon}',\boldsymbol{\epsilon},\omega)=\Sigma_{\alpha\alpha'}\epsilon'_\alpha\epsilon_{\alpha'}M_{\alpha\alpha'}(j,\omega)$, we rewrite Eq. (2.2) as

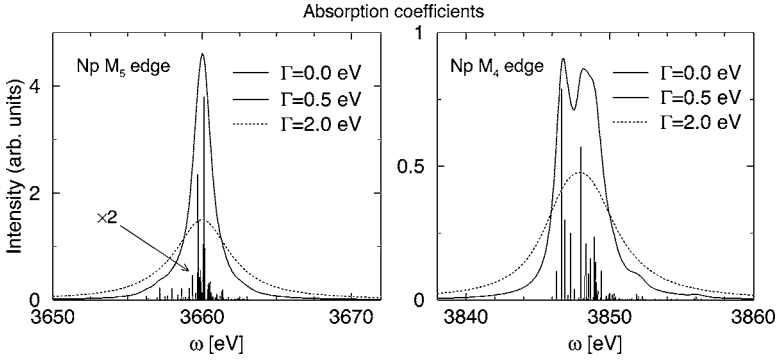


FIG. 7. Absorption coefficients as functions of the photon energy at the Np $M_4$ (right panel) and $M_5$ (left panel) edges. The bold solid and dotted lines represent the calculated results for $\Gamma=0.5$ and 2.0 eV, respectively. The vertical bars represent $\delta$ functions with $\Gamma=0$.

TABLE IV. Antisymmetric matrices, $M^x$, $M^y$, $M^z$, and symmetric matrices $M^{yz}$, $M^{zx}$, $M^{xy}$, $M^{3z^2-r^2}$, $M^{x^2-y^2}$.

| | | | | | |
|---|---|---|---|---|---|
| Antisymmetric | $M^x$ | $M^y$ | $M^z$ | | |
| | $\begin{pmatrix} 0 & 0 & 0 \\ 0 & 0 & 1 \\ 0 & -1 & 0 \end{pmatrix}$ | $\begin{pmatrix} 0 & 0 & -1 \\ 0 & 0 & 0 \\ 1 & 0 & 0 \end{pmatrix}$ | $\begin{pmatrix} 0 & 1 & 0 \\ -1 & 0 & 0 \\ 0 & 0 & 0 \end{pmatrix}$ | | |
| Symmetric | $M^{yz}$ | $M^{zx}$ | $M^{xy}$ | $M^{3z^2-r^2}$ | $M^{x^2-y^2}$ |
| | $\begin{pmatrix} 0 & 0 & 0 \\ 0 & 0 & 1 \\ 0 & 1 & 0 \end{pmatrix}$ | $\begin{pmatrix} 0 & 0 & 1 \\ 0 & 0 & 0 \\ 1 & 0 & 0 \end{pmatrix}$ | $\begin{pmatrix} 0 & 1 & 0 \\ 1 & 0 & 0 \\ 0 & 0 & 0 \end{pmatrix}$ | $\begin{pmatrix} -1 & 0 & 0 \\ 0 & -1 & 0 \\ 0 & 0 & 2 \end{pmatrix}$ | $\begin{pmatrix} 1 & 0 & 0 \\ 0 & -1 & 0 \\ 0 & 0 & 0 \end{pmatrix}$ |

$$M_{\alpha\alpha'}(j,\omega) = \sum_{J',M,i} E_i(\omega,J')\langle\psi_0|x_{\alpha,j}|J',M,i\rangle \times \langle J',M,i|x_{\alpha',j}|\psi_0\rangle, \tag{A1}$$

with

$$E_i(\omega,J') = \frac{1}{\hbar\omega - (E_{J',i} - E_0) + i\Gamma}. \tag{A2}$$

Assuming that the ground-state wave function is expressed as a linear combination of $|J,m\rangle$ at each site,

$$|\psi_0\rangle = \sum_m c_j(m)|J,m\rangle, \tag{A3}$$

and inserting this equation into Eq. (A1), we obtain

$$M_{\alpha\alpha'}(j,\omega) = \sum_{m,m'} c_j^*(m)c_j(m')M_{\alpha\alpha'}^{m,m'}(\omega), \tag{A4}$$

with

$$M_{\alpha\alpha'}^{m,m'}(\omega) = \sum_{J'}\sum_{i=1}^{N_{J'}} E_i(\omega,J') \sum_{M=-J'}^{J'} \langle J,m|x_\alpha|J',M,i\rangle \times\langle J',M,i|x_{\alpha'}|J,m'\rangle, \tag{A5}$$

where the number of the multiplets having the value $J$ is denoted by $N_J$. We have suppressed the index $j$ specifying the core-hole site. The selection rule for the $E1$ process confines the range of the summation over $J'$ to $J'=J,J\pm1$. The matrix element of the type $\langle J,m|x_\alpha|J',M\rangle$ is analyzed by utilizing the Wigner-Eckart theorem for a vector operator with the use of the Wigner's $3j$ symbol:[49]

$$\langle J,m|s_\mu|J'M\rangle = (-1)^{J'+m-1}\sqrt{2J+1}\begin{pmatrix} J' & 1 & J \\ M & \mu & -m \end{pmatrix}(J\|V_1\|J'), \tag{A6}$$

with $s_{\pm1} = \mp(1/\sqrt{2})(x\pm iy)$, $s_0=z$. The symbol $(J\|V_1\|J')$ denotes the reduced matrix element of the set of irreducible tensor operator of the first rank. Because of the nature of the dipole operators, $M^{m,m'}(\omega)\neq\mathbf{0}$ only when $|m-m'|\leqslant 2$. After lengthy calculation, we obtain

$$M_{\alpha,\alpha'}^{m,m}(\omega) = -\frac{3}{4}\left[\frac{1}{3}J(J+1) - m^2\right]\alpha_2(\omega)M_{\alpha,\alpha'}^{3z^2-r^2} - \mathrm{i}m\alpha_1(\omega)M_{\alpha,\alpha'}^{z} + \alpha_0(\omega)\delta_{\alpha,\alpha'}, \tag{A7a}$$

$$M_{\alpha,\alpha'}^{m,m+1}(\omega) = \frac{3}{8}f_m(2m+1)\alpha_2(\omega)(M^{zx}+\mathrm{i}M^{yz})_{\alpha,\alpha'} - \mathrm{i}\frac{1}{2}f_m\alpha_1(\omega)(M^{x}+\mathrm{i}M^{y})_{\alpha,\alpha'}, \tag{A7b}$$

$$M_{\alpha,\alpha'}^{m+1,m}(\omega) = \frac{3}{8}f_m(2m+1)\alpha_2(\omega)(M^{zx}-\mathrm{i}M^{yz})_{\alpha,\alpha'} - \mathrm{i}\frac{1}{2}f_m\alpha_1(\omega)(M^{x}-\mathrm{i}M^{y})_{\alpha,\alpha'}, \tag{A7c}$$

$$M_{\alpha,\alpha'}^{m,m+2}(\omega) = a_m''\alpha_2(\omega)(M^{x^2-y^2}+\mathrm{i}M^{xy})_{\alpha,\alpha'}, \tag{A7d}$$

$$M_{\alpha,\alpha'}^{m+2,m}(\omega) = a_m''\alpha_2(\omega)(M^{x^2-y^2}-\mathrm{i}M^{xy})_{\alpha,\alpha'}, \tag{A7e}$$

where

$$f_m = \sqrt{(J-m)(J+m+1)}, \tag{A8}$$

$$a_m'' = \frac{3}{8}f_m f_{m+1}, \tag{A9}$$

and the $3\times3$ matrices, $M^x$, $M^y$, $M^z$, $M^{xy}$, $M^{yz}$, $M^{zx}$, $M^{x^2-y^2}$, and $M^{3z^2-r^2}$ are tabulated in Table IV. The energy profiles are given by

$$\alpha_0(\omega) = \frac{2}{3}J(2J-1)F_{J-1}(\omega) + \frac{2}{3}J(J+1)F_J(\omega) + \frac{2}{3}(2J^2+5J+3)F_{J+1}(\omega), \tag{A10a}$$

$$\alpha_1(\omega) = -(2J-1)F_{J-1}(\omega) - F_J(\omega) + (2J+3)F_{J+1}(\omega), \tag{A10b}$$

$$\alpha_2(\omega) = \frac{4}{3}[-F_{J-1}(\omega) + F_J(\omega) - F_{J+1}(\omega)], \tag{A10c}$$

with

$$F_{J'}(\omega) = 2^{1-|J-J'|}\sqrt{(2J+1)(2J'+1)}\frac{(J+J'-1)!}{(J+J'+2)!} \times |(J\|V_1\|J')|^2 \sum_{i=1}^{N_{J'}} E_i(\omega, J'). \tag{A11}$$

Substituting Eqs. (A7) into Eq. (A4), we obtain the final expression, Eq. (2.3).


[1] Y. Murakami *et al.*, Phys. Rev. Lett. **81**, 582 (1998).
[2] S. Ishihara and S. Maekawa, Phys. Rev. Lett. **80**, 3799 (1998).
[3] I. S. Elfimov, V. I. Anisimov, and G. A. Sawatzky, Phys. Rev. Lett. **82**, 4264 (1999).
[4] M. Benfatto, Y. Joly, and C. R. Natoli, Phys. Rev. Lett. **83**, 636 (1999).
[5] M. Takahashi, J. Igarashi, and P. Fulde, J. Phys. Soc. Jpn. **68**, 2530 (1999).
[6] E. D. Isaacs, D. B. McWhan, R. N. Kleiman, D. J. Bishop, G. E. Ice, P. Zschack, B. D. Gaulin, T. E. Mason, J. D. Garrett, and W. J. L. Buyers, Phys. Rev. Lett. **65**, 3185 (1990).
[7] D. Mannix, G. H. Lander, J. Rebizant, R. Caciuffo, N. Bernhoeft, E. Lidström, and C. Vettier, Phys. Rev. B **60**, 15187 (1999).
[8] M. J. Longfield, J. A. Paixão, N. Bernhoeft, G. H. Lander, F. Wastin, and J. Rebizant, Phys. Rev. B **66**, 134421 (2002).
[9] J. P. Hannon, G. T. Trammell, M. Blume, and D. Gibbs, Phys. Rev. Lett. **61**, 1245 (1988); **62**, 2644(E) (1989).
[10] D. W. Osborne and J. E. F. Westrum, J. Chem. Phys. **21**, 1884 (1953).
[11] P. Erdös, G. Solt, Z. Żołnierek, A. Blaise, and J. M. Fournier, Physica B & C **102**, 164 (1980).
[12] B. D. Dunlap, G. M. Kalvius, D. J. Lam, and B. Brodsky, J. Phys. Chem. Solids **29**, 1365 (1968).
[13] J. M. Friedt, F. J. Litterst, and J. Rebizant, Phys. Rev. B **32**, 257 (1985).
[14] D. E. Cox and B. Frazer, J. Phys. Chem. Solids **28**, 1649 (1967).
[15] L. Heaton, M. H. Mueller, and J. M. Williams, J. Phys. Chem. Solids **28**, 1651 (1967).
[16] J. W. Ross and D. J. Lam, J. Appl. Phys. **38**, 1451 (1967).
[17] W. Kopmann, F. J. Litterst, H. H. Klauß, M. Hillberg, W. Wagener, G. M. Kalvius, E. Schreier, F. J. Burghart, J. Rebizant, and G. H. Lander, J. Alloys Compd. **271-273**, 463 (1998).
[18] P. Santini and G. Amoretti, Phys. Rev. Lett. **85**, 2188 (2000); **85**, 5481(E) (2000).
[19] P. Santini and G. Amoretti, J. Phys. Soc. Jpn. **71**, 11 (2002).
[20] J. A. Paixão, C. Detlefs, M. J. Longfield, R. Caciuffo, P. Santini, N. Bernhoeft, J. Rebizant, and G. H. Lander, Phys. Rev. Lett. **89**, 187202 (2002).
[21] Y. Tokunaga, Y. Homma, S. Kambe, D. Aoki, H. Sakai, E. Yamamoto, A. Nakamura, Y. Shiokawa, R. E. Walstedt, and H. Yasuoka, Phys. Rev. Lett. **94**, 137209 (2005).
[22] A. Kiss and P. Fazekas, Phys. Rev. B **68**, 174425 (2003).
[23] K. Kubo and T. Hotta, Phys. Rev. B **71**, 140404(R) (2005).
[24] R. Caciuffo, J. A. Paixão, M. J. Longfield, P. Santini, N. Bernhoeft, and G. H. Lander, J. Phys.: Condens. Matter **15**, S2287 (2003).
[25] M. Blume, J. Appl. Phys. **57**, 3615 (1985).
[26] M. Blume and D. Gibbs, Phys. Rev. B **37**, 1779 (1988).
[27] J. P. Hill and D. F. McMorrow, Acta Crystallogr., Sect. A: Found. Crystallogr. **52**, 236 (1996).
[28] A. Delapalme, M. Forte, J. M. Fournier, J. Rebizant, and J. C. Spirlet, Physica B & C **102**, 171 (1980).
[29] R. Cowan, *The Theory of Atomic Structure and Spectra* (University of California Press, Berkeley, 1981).
[30] A. V. Nikolaev, Phys. Rev. B **71**, 165102 (2005).
[31] T. Nagao and J. Igarashi, J. Phys. Soc. Jpn. **72**, 2381 (2003).
[32] G. Amoretti, A. Blaise, R. Caciuffo, D. Cola, J. M. Fournier, M. T. Hutchings, G. H. Lander, R. Osborn, A. Severing, and A. D. Taylor, J. Phys.: Condens. Matter **4**, 3459 (1992).
[33] Our definition of the CEF parameters $B_4$ and $B_6$ is different from that of Amoretti's, $V_4$ and $V_6$ in Eq. (31) of Ref. 32. They are related as $B_4=\beta V_4$ and $B_6=\gamma V_6$ where $\beta$ and $\gamma$ are the Stevens' multiplicative factors of the $f^3$ configuration.
[34] R. Shiina, H. Shiba, and P. Thalmeier, J. Phys. Soc. Jpn. **66**, 1741 (1997).
[35] S. W. Lovesey, E. Balcar, C. Deltefs, G. van der Laan, D. S. Sivia, and U. Staub, J. Phys.: Condens. Matter **15**, 4511 (2003).
[36] S. B. Wilkins, J. A. Paixão, R. Caciuffo, P. Javorsky, F. Wastin, J. Rebizant, C. Detlefs, N. Bernhoeft, P. Santini, and G. H. Lander, Phys. Rev. B **70**, 214402 (2004).
[37] A. V. Nikolaev and K. H. Michel, Phys. Rev. B **68**, 054112 (2003).
[38] H. Nakao, K. Magishi, Y. Wakabayashi, Y. Murakami, K. Koyama, K. Hirota, Y. Endoh, and S. Kunii, J. Phys. Soc. Jpn. **70**, 1857 (2001).
[39] F. Yakhou, V. Plakhty, H. Suzuki, S. Gavrilov, P. Burlet, L. Paolasini, C. Vettier, and S. Kunii, Phys. Lett. A **285**, 191 (2001).
[40] Y. Tanaka, T. Inami, T. Nakamura, H. Yamauchi, H. Onodera, K. Ohyama, and Y. Yamaguchi, J. Phys.: Condens. Matter **11**, L505 (1999).
[41] K. Hirota, N. Oumi, T. Matsumura, H. Nakao, Y. Wakabayashi, Y. Murakami, and Y. Endoh, Phys. Rev. Lett. **84**, 2706 (2000).
[42] T. Matsumura, D. Okuyama, N. Oumi, K. Hirota, H. Nakao, Y. Murakami, and Y. Wakabayashi, J. Phys. Soc. Jpn. **74**, 1500 (2005).
[43] T. Nagao and J. Igarashi, J. Phys. Soc. Jpn. **70**, 2892 (2001).
[44] J. Igarashi and T. Nagao, J. Phys. Soc. Jpn. **71**, 1771 (2002).
[45] J. Igarashi and T. Nagao, J. Phys. Soc. Jpn. **72**, 1279 (2003).
[46] J. Luo, G. T. Trammell, and J. P. Hannon, Phys. Rev. Lett. **71**, 287 (1993).
[47] S. W. Lovesey and E. Balcar, J. Phys.: Condens. Matter **8**, 10983 (1996).
[48] T. Nagao and J. Igarashi, J. Phys. Soc. Jpn. **74**, 765 (2005).
[49] M. Tinkham, *Group Theory and Quantum Mechanics* (McGraw-Hill, New York, 1964).